

# **Supplementary material for "Dynamic mode decomposition of random pressure fields over bluff bodies", Part 1**

This is the supplementary material for the paper entitled "Dynamics of random pressure fields over bluff bodies: a dynamic mode decomposition perspective". In this paper, an operator-theoretic method is introduced to a dynamical system analysis involving transient mapping of pressure fluctuations around a prism surface immersed in a turbulent boundary layer. Compared to the state-space method, the operator-theoretic modeling characterizes the evolution mechanism via an infinite-dimensional linear operator, i.e. nonlinear dynamics is linearized in the entire basin without sacrificing computational accuracy. This is accomplished by the spectral analysis of the Koopman operator, which lifts a dynamical system from phase space to Hilbert function space. In particular, the dynamic mode decomposition (DMD) is used to obtain the Koopman eigen-tuple. The proposed system decomposition scheme has been demonstrated using random aerodynamic pressure fields over the surface of a scaled model of a finite height prism. To improve the algorithm's performance, Takens's embedding theorem is incorporated into the learning scheme, thus reinforcing the dynamical mechanisms buried in data with a noisy background.

A comparative study between classical POD and proposed augmented DMD is carried out using a high-dimensional random pressure field, which is continually evolving in time through a differential operator. The POD is limited to producing a set of hierarchically structured eigenmodes in terms of the time-averaged spatial tensor, and each mode is randomly evolving in time. On the contrary, the DMD representation is spatiotemporally orthogonal where each identified coherent structure is assigned to a specific frequency and a corresponding temporal growth/decay. The results are summarized as follows.

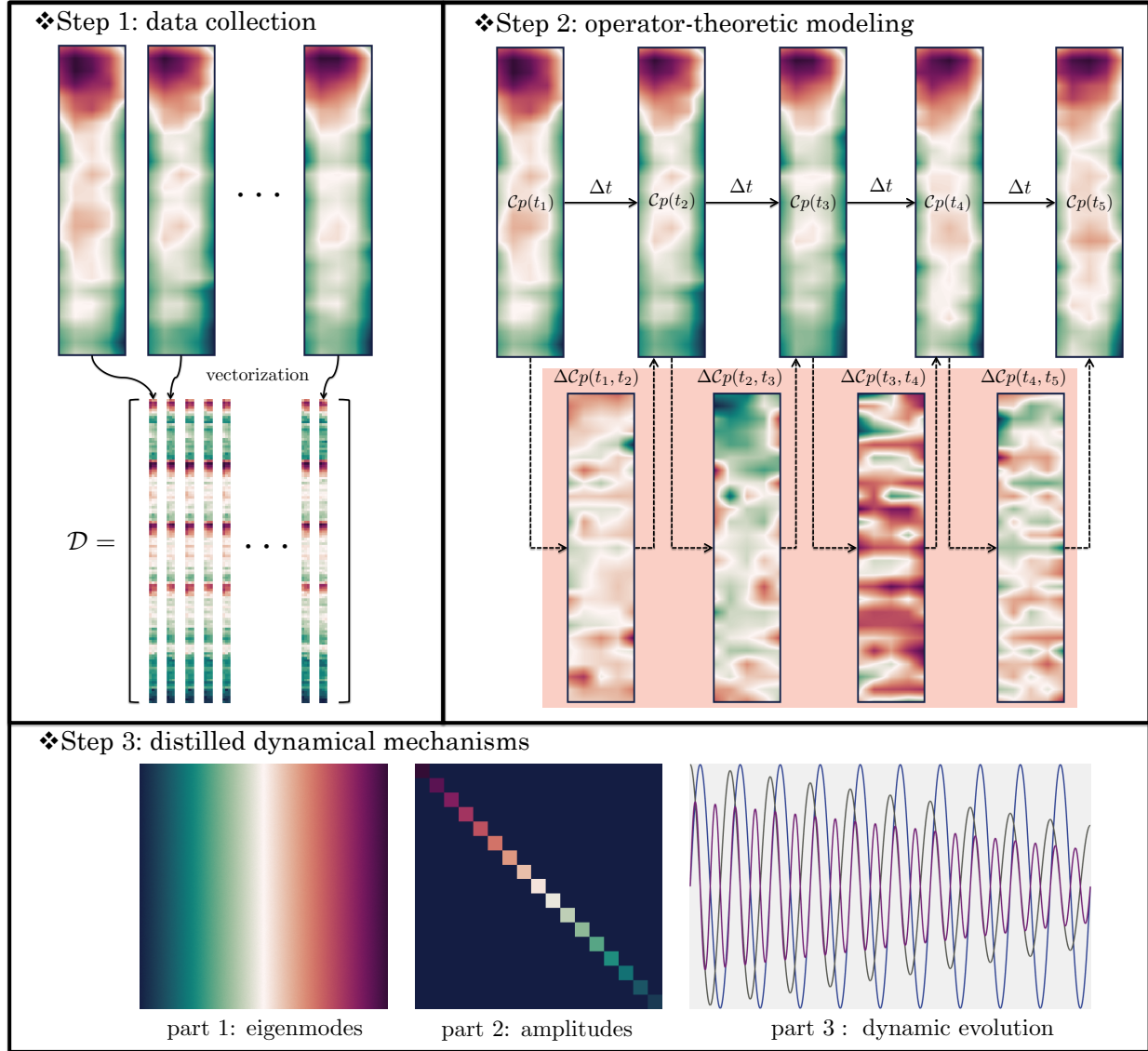
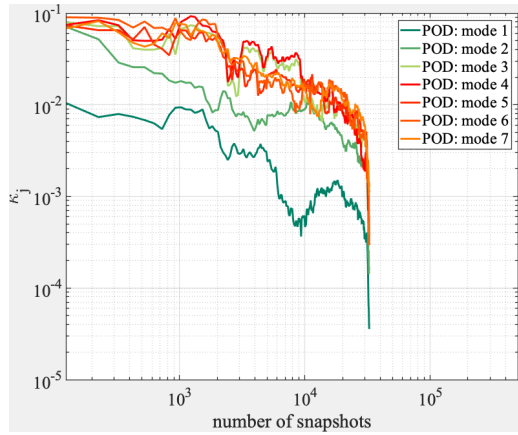
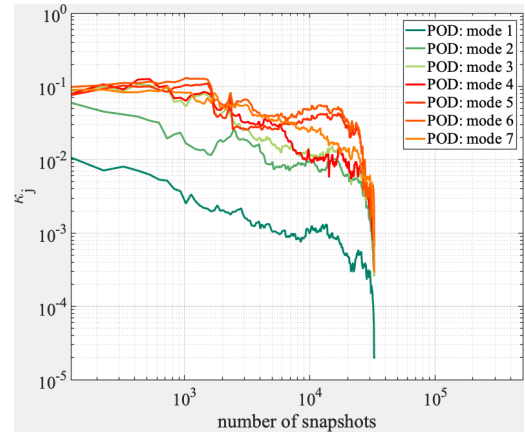


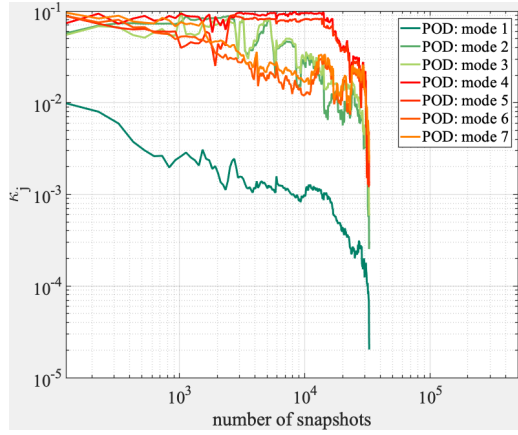
Figure 1: Schematic overview of the proposed equation-free learning with application to the random aerodynamic pressure field. The overall procedure contains three steps: (1) data collection, (2) operator-theoretic modeling, and (3) dynamics interpretation.



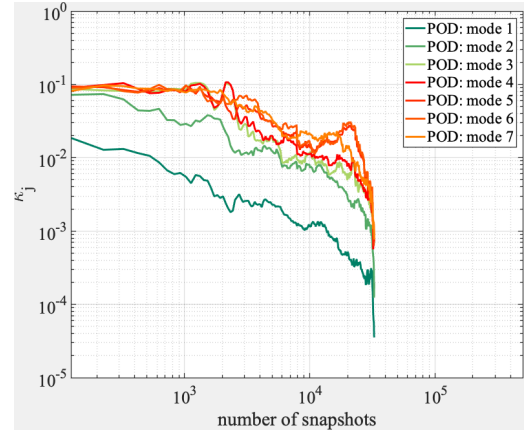
(a.1) Windward scenario: POD eigenmodes



(a.2) Leftside scenario: POD eigenmodes

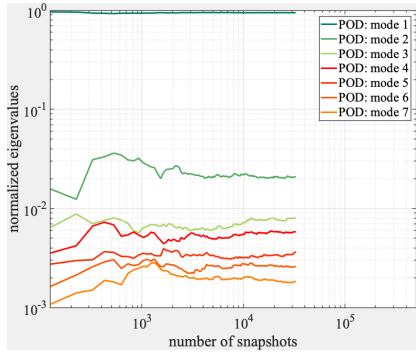


(a.3) Leeward scenario: POD eigenmodes

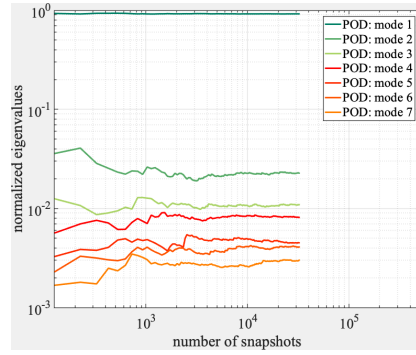


(a.4) Rightside scenario: POD eigenmodes

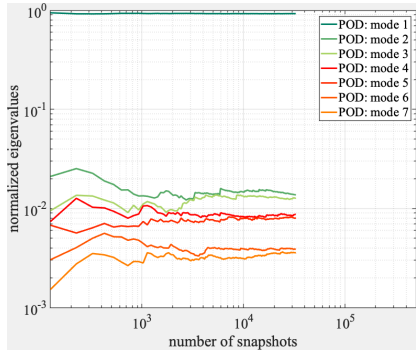
Figure 2: Convergence analysis of POD modes.



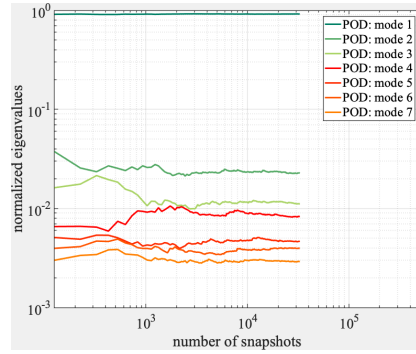
(a.1) Windward scenario: normalized POD eigenvalues



(a.2) Leftside scenario: normalized POD eigenvalues

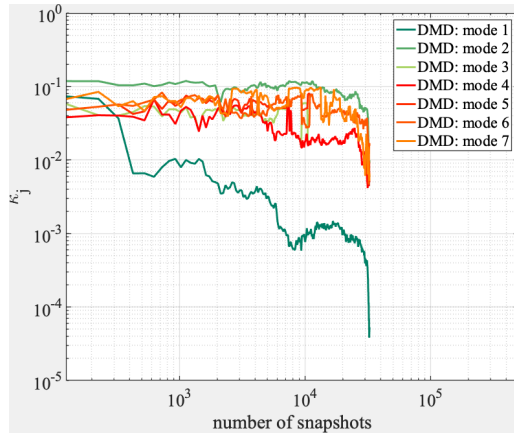


(a.3) Leeward scenario: normalized POD eigenvalues

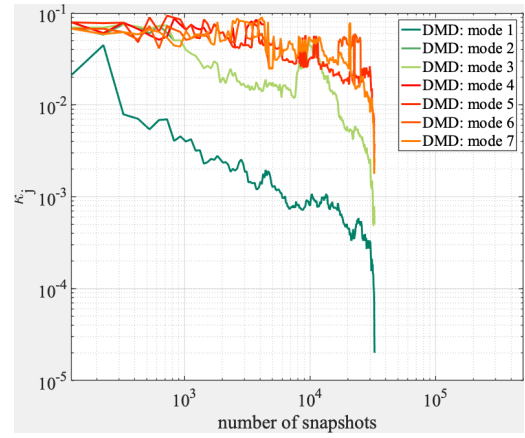


(a.4) Rightside scenario: normalized POD eigenvalues

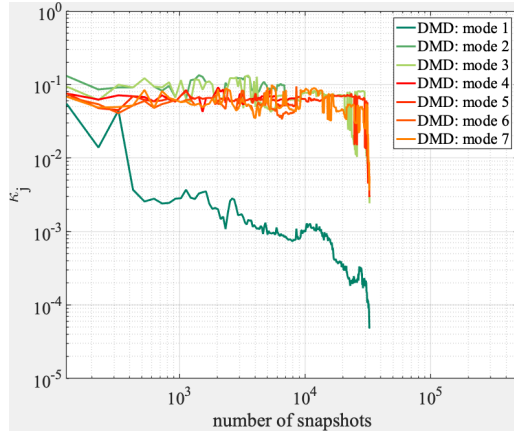
Figure 3: Convergence analysis of normalized POD eigenvalues.



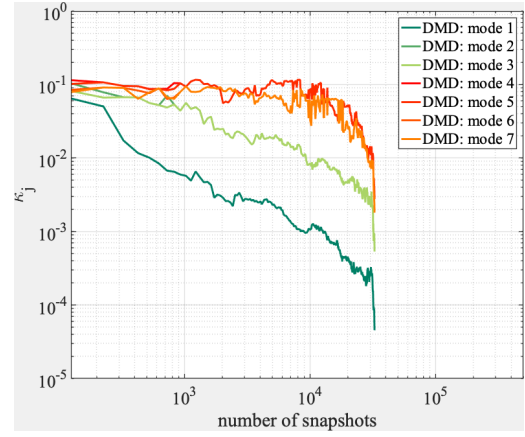
(a.1) Windward scenario: DMD eigenmodes



(a.2) Leftside scenario: DMD eigenmodes

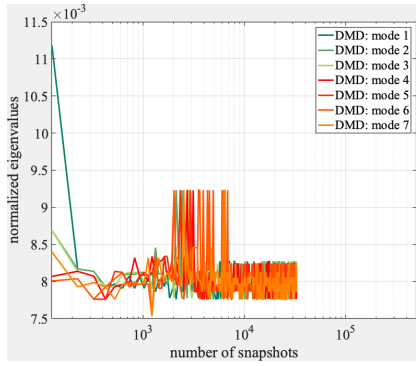


(a.3) Leeward scenario: DMD eigenmodes

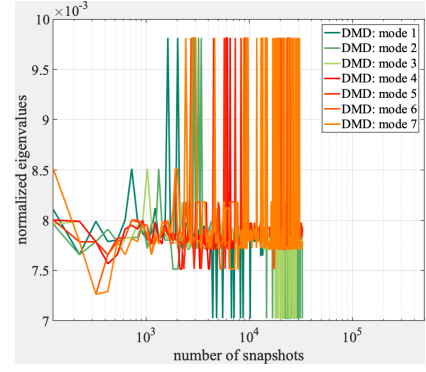


(a.4) Rightside scenario: DMD eigenmodes

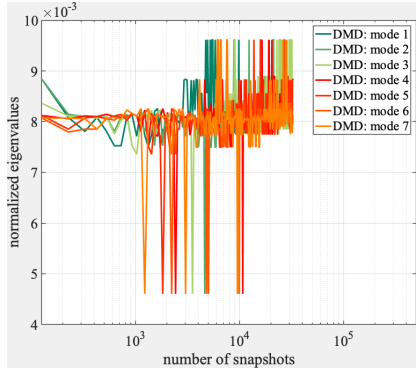
Figure 4: Convergence analysis of DMD modes.



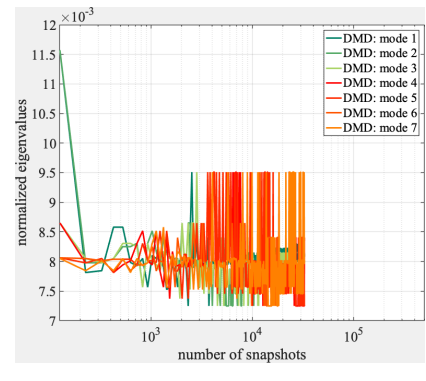
(a.1) Windward scenario: normalized DMD eigenvalues



(a.2) Leftside scenario: normalized DMD eigenvalues



(a.3) Leeward scenario: normalized DMD eigenvalues



(a.4) Rightside scenario: normalized DMD eigenvalues

Figure 5: Convergence analysis of normalized DMD eigenvalues.

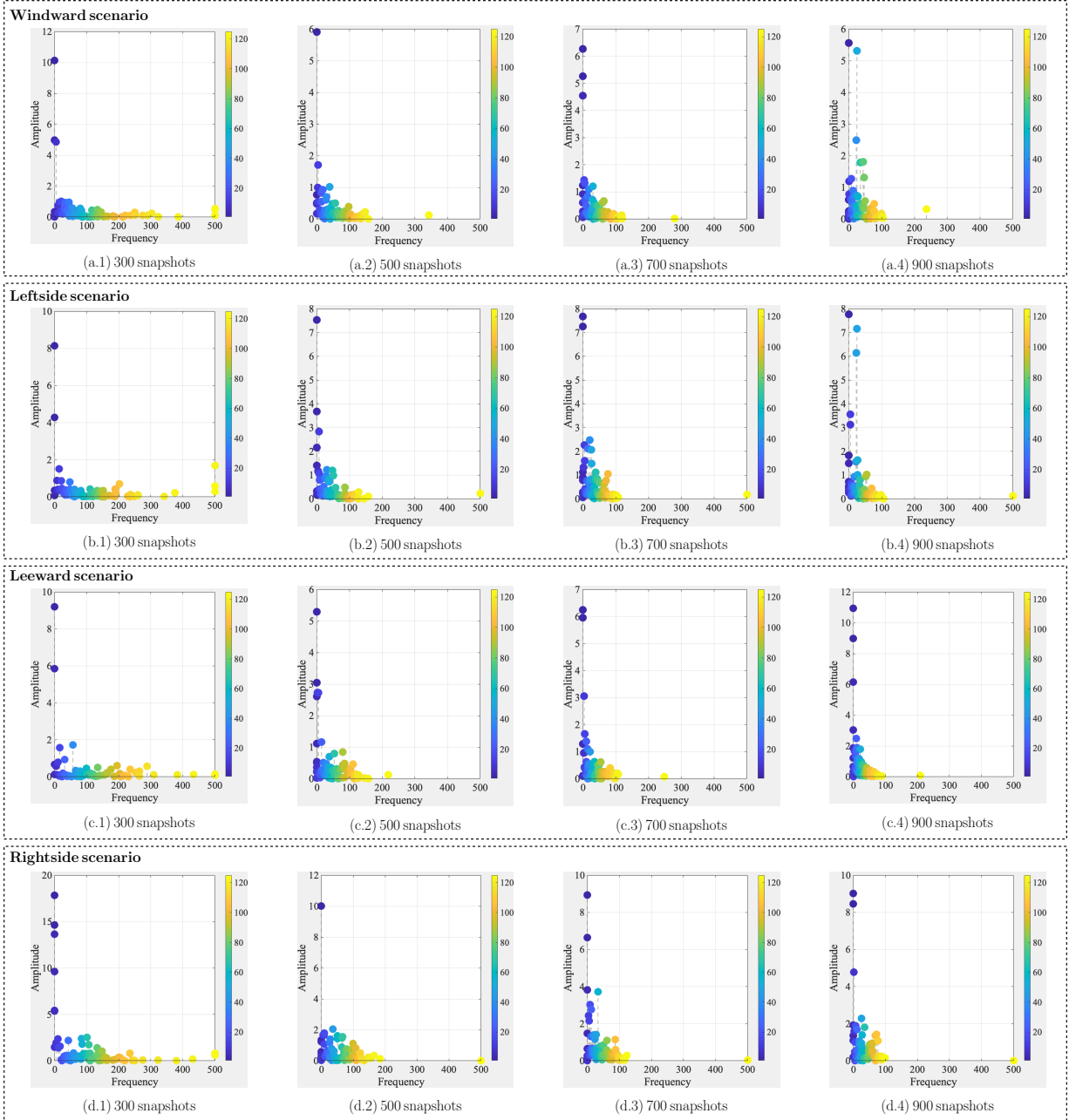


Figure 6: Convergence analysis of DMD energy spectra.

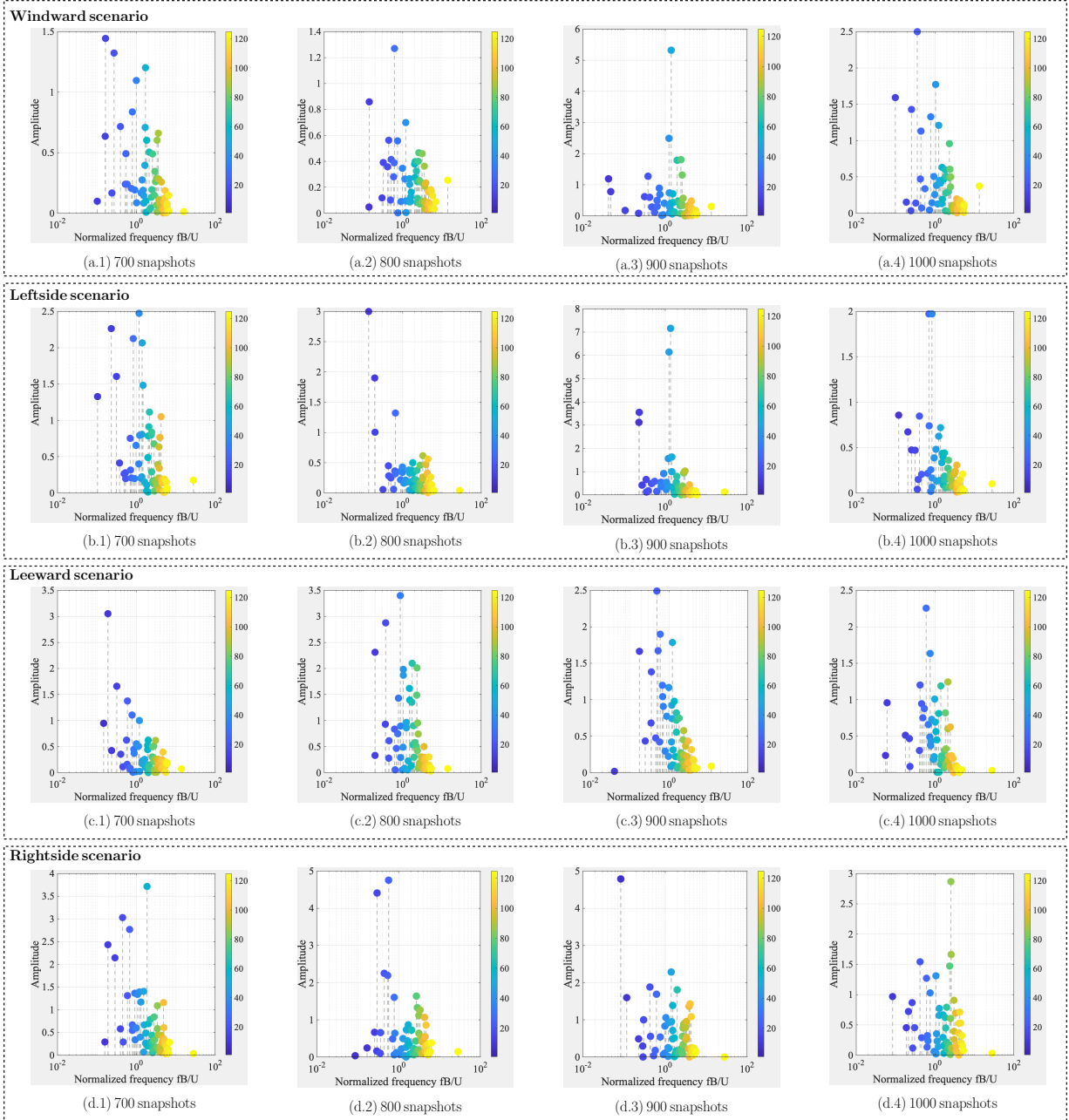
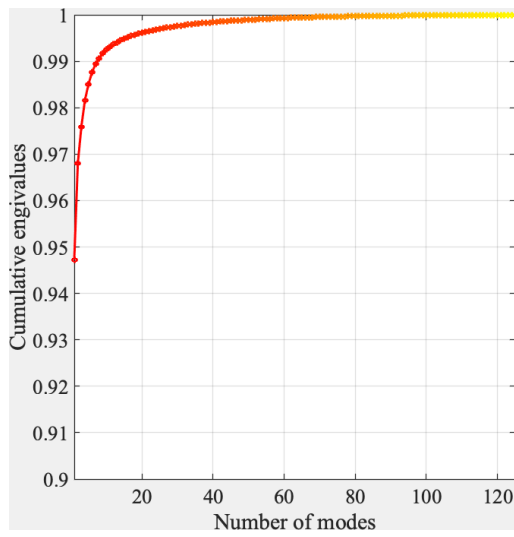
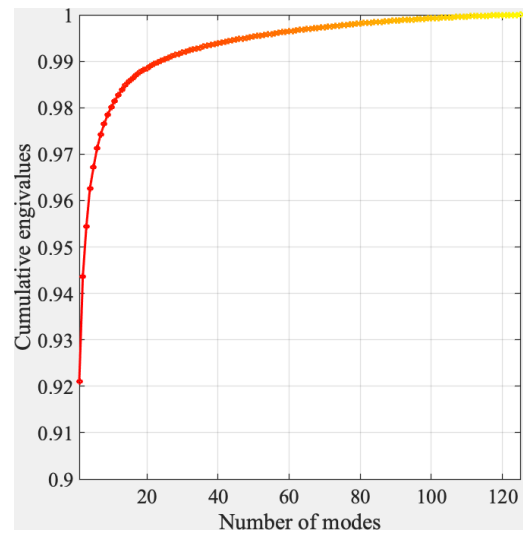


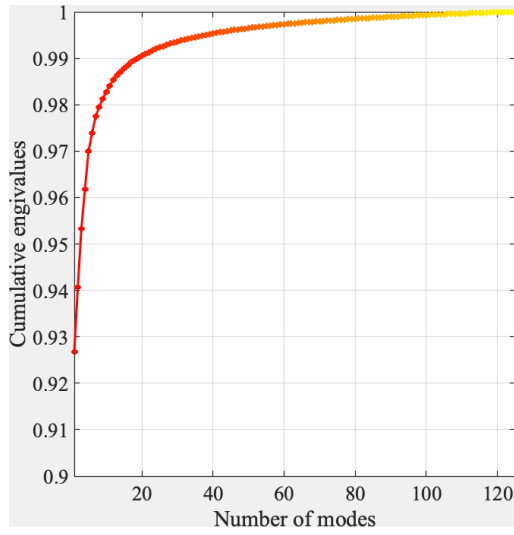
Figure 7: Illustration of different dynamics manifestations inherent in the converged frequency band, where dynamics is a function of  $N_{snap}$ .



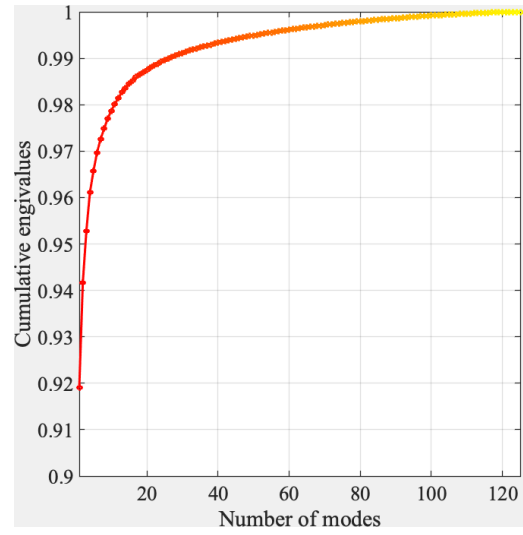
(a.1) Windward scenario: original dataset  $\mathcal{D}$



(a.2) Leftside scenario: original dataset  $\mathcal{D}$

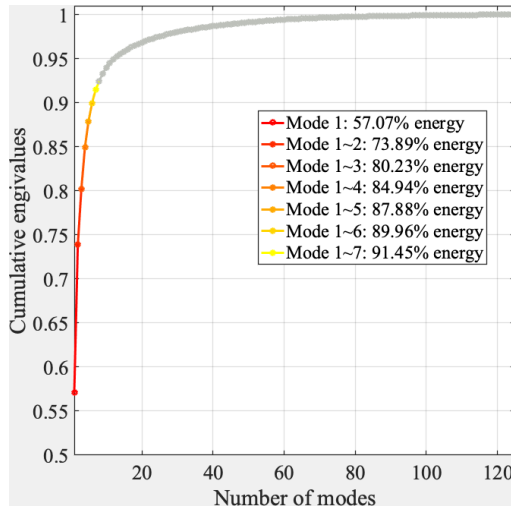


(a.3) Leeward scenario: original dataset  $\mathcal{D}$

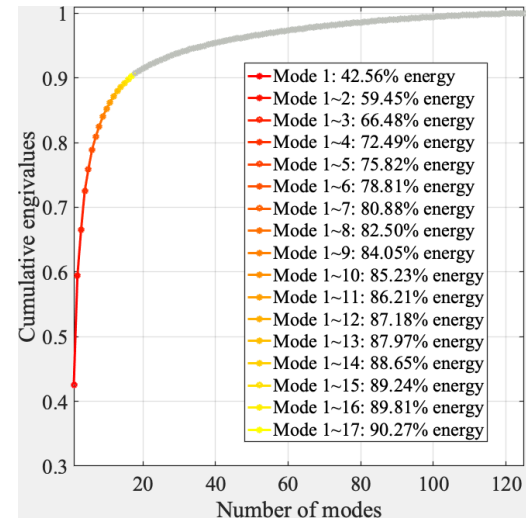


(a.4) Rightside scenario: original dataset  $\mathcal{D}$

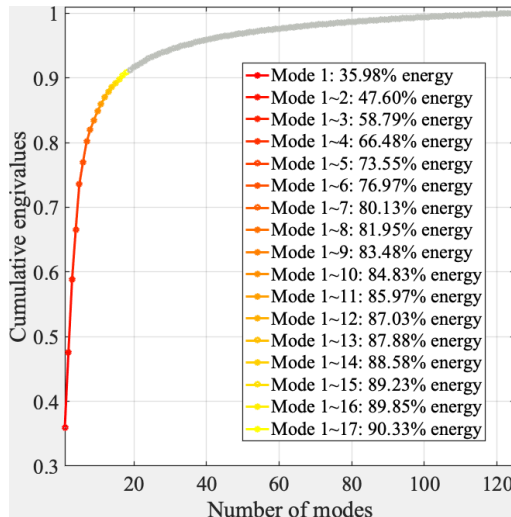
Figure 8: Cumulative eigenvalues versus the number of POD modes. Dataset  $\mathcal{D}$



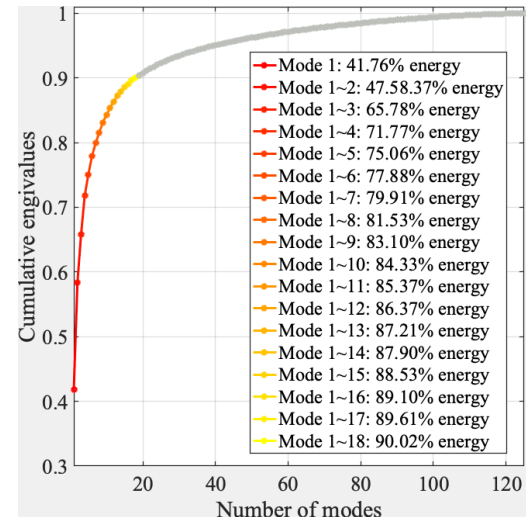
(a.1) Windward scenario: dataset  $\mathcal{D} - \bar{\mathcal{D}}$



(a.2) Leftside scenario: dataset  $\mathcal{D} - \bar{\mathcal{D}}$



(a.3) Leeward scenario: dataset  $\mathcal{D} - \bar{\mathcal{D}}$



(a.4) Rightside scenario: dataset  $\mathcal{D} - \bar{\mathcal{D}}$

Figure 9: Cumulative eigenvalues versus the number of POD modes. Dataset  $\mathcal{D} - \bar{\mathcal{D}}$

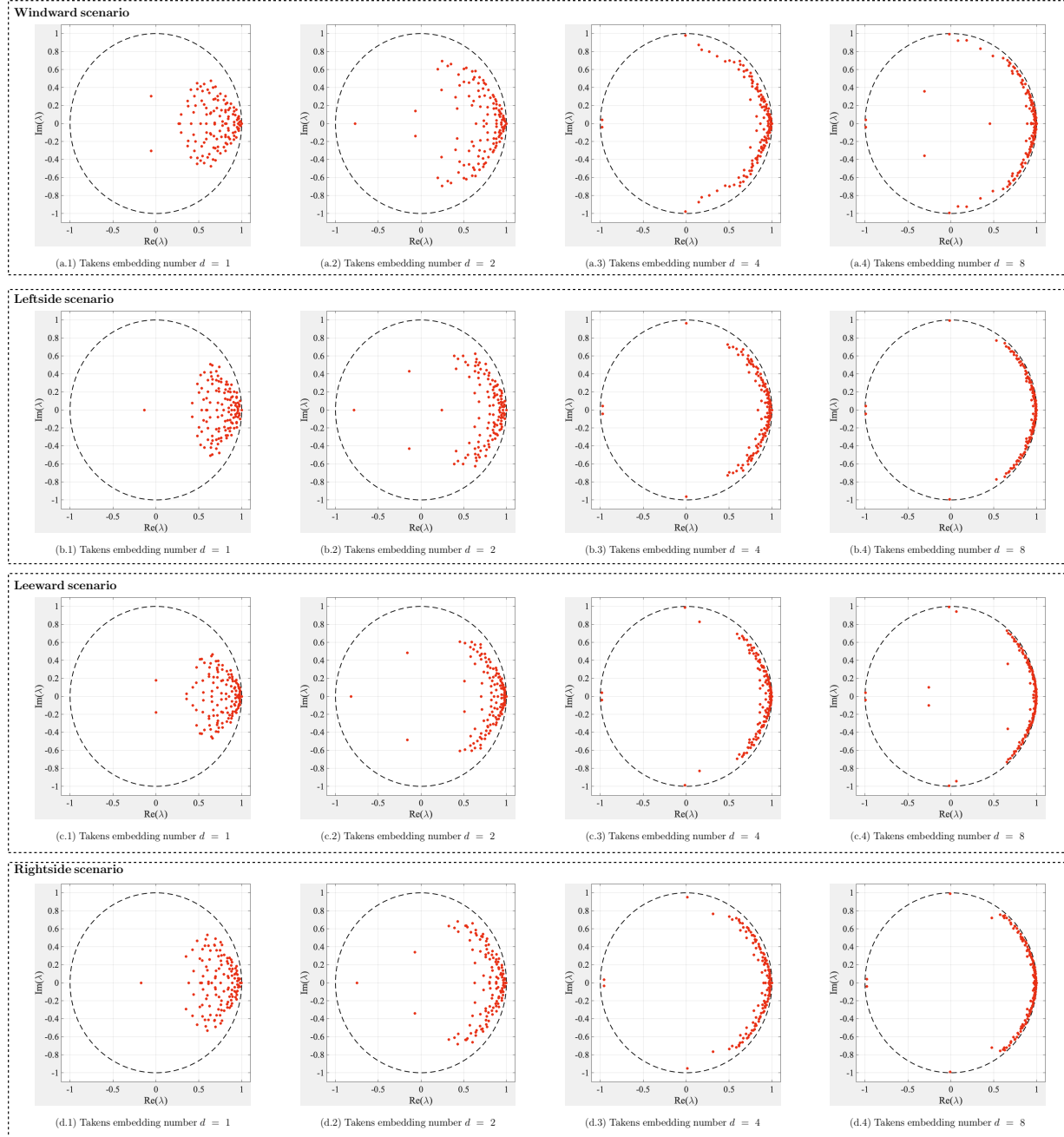


Figure 10: Scatterplot of the DMD eigenvalues.

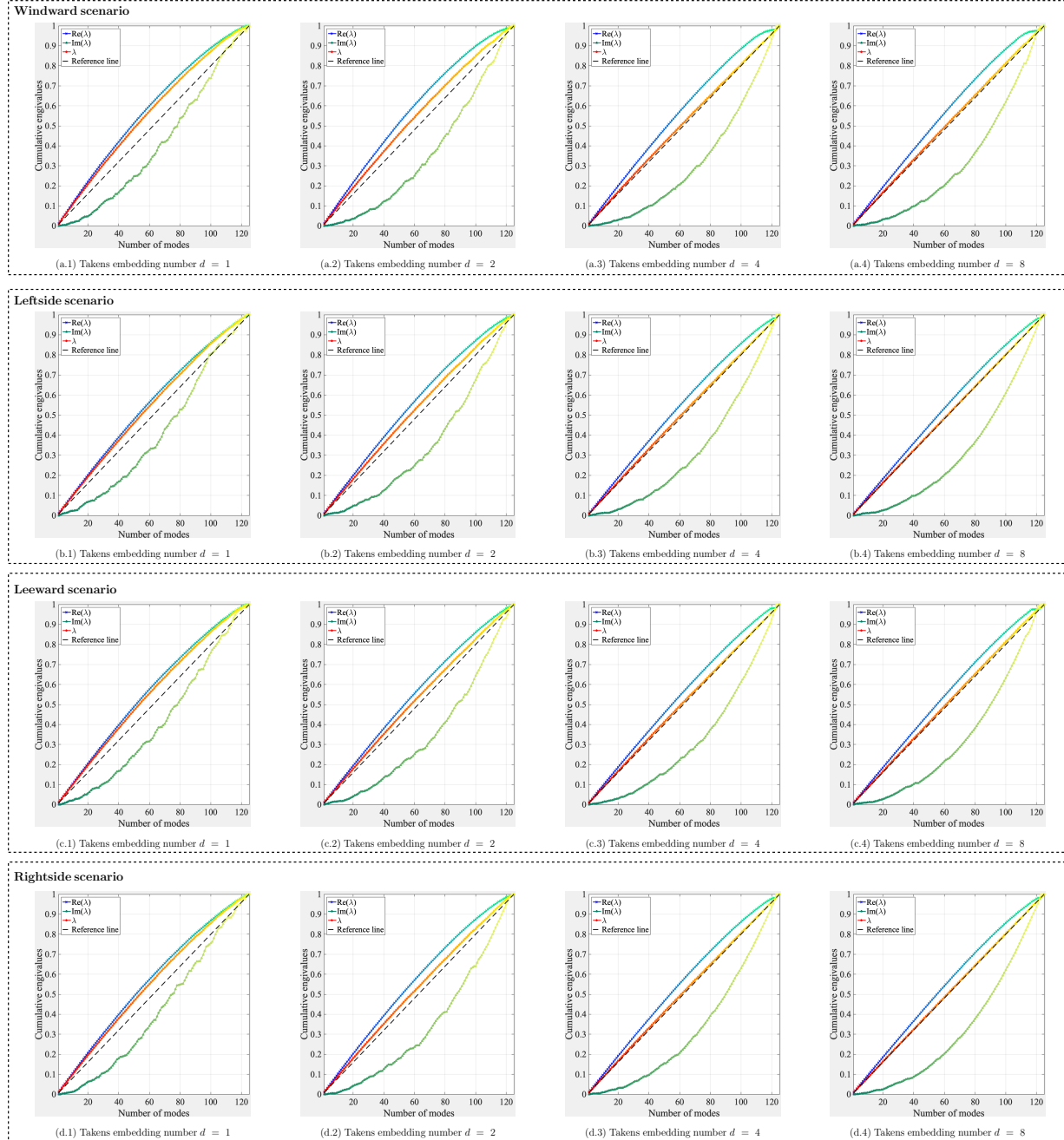


Figure 11: Cumulative eigenvalues versus the number of DMD modes. The straight reference line is a linear function whose independent variable is the number of DMD modes, the dependent variable is the normalized cumulative eigenvalues, and the intercept is 0.

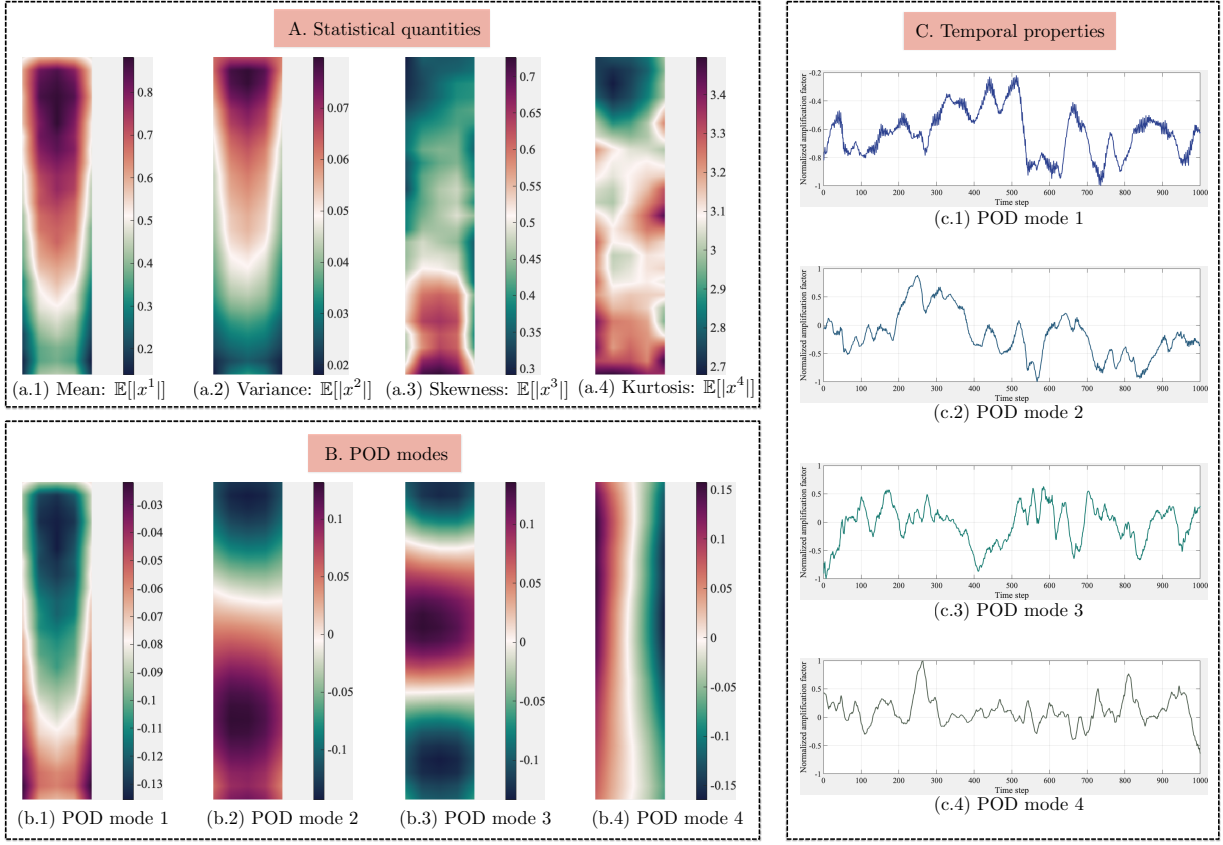


Figure 12: Windward scenario: the decomposed spatial and temporal tensor by the POD algorithm.

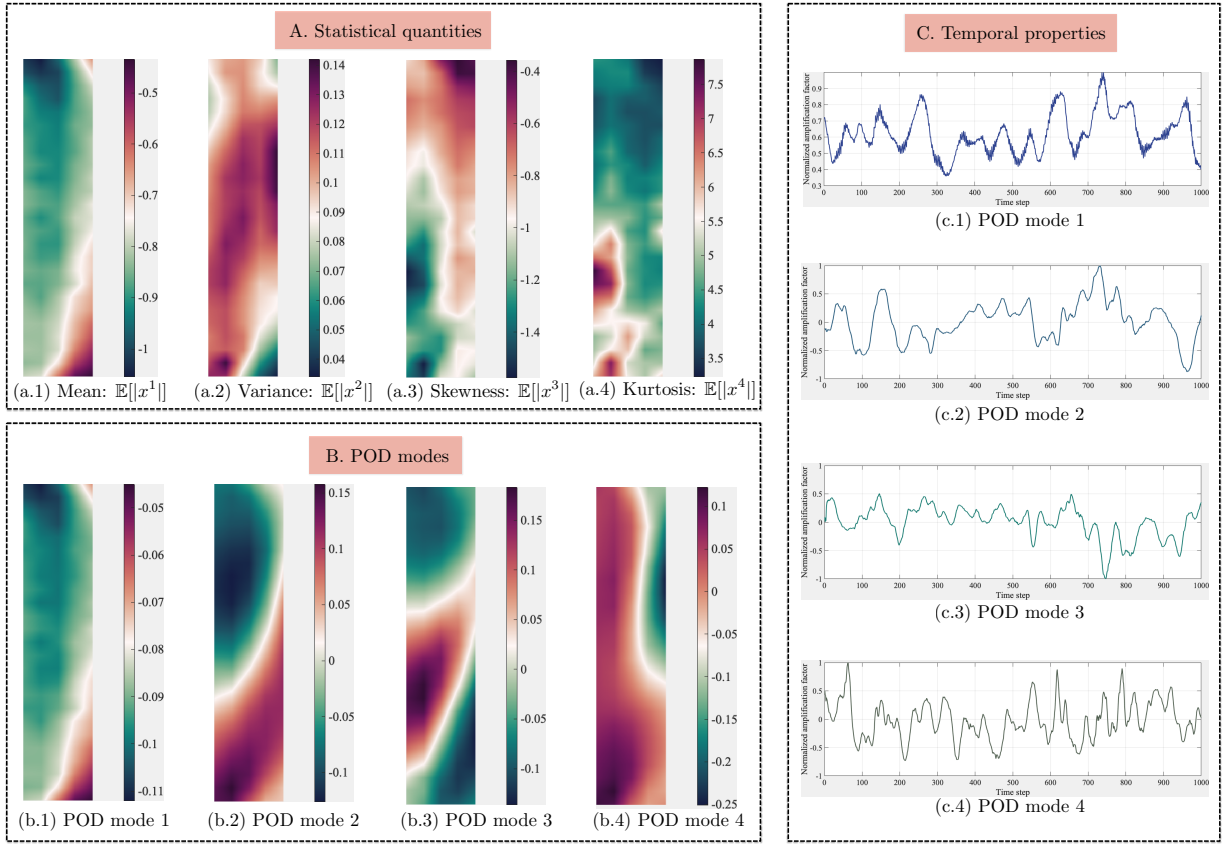


Figure 13: Leftside scenario: the decomposed spatial and temporal tensor by the POD algorithm.

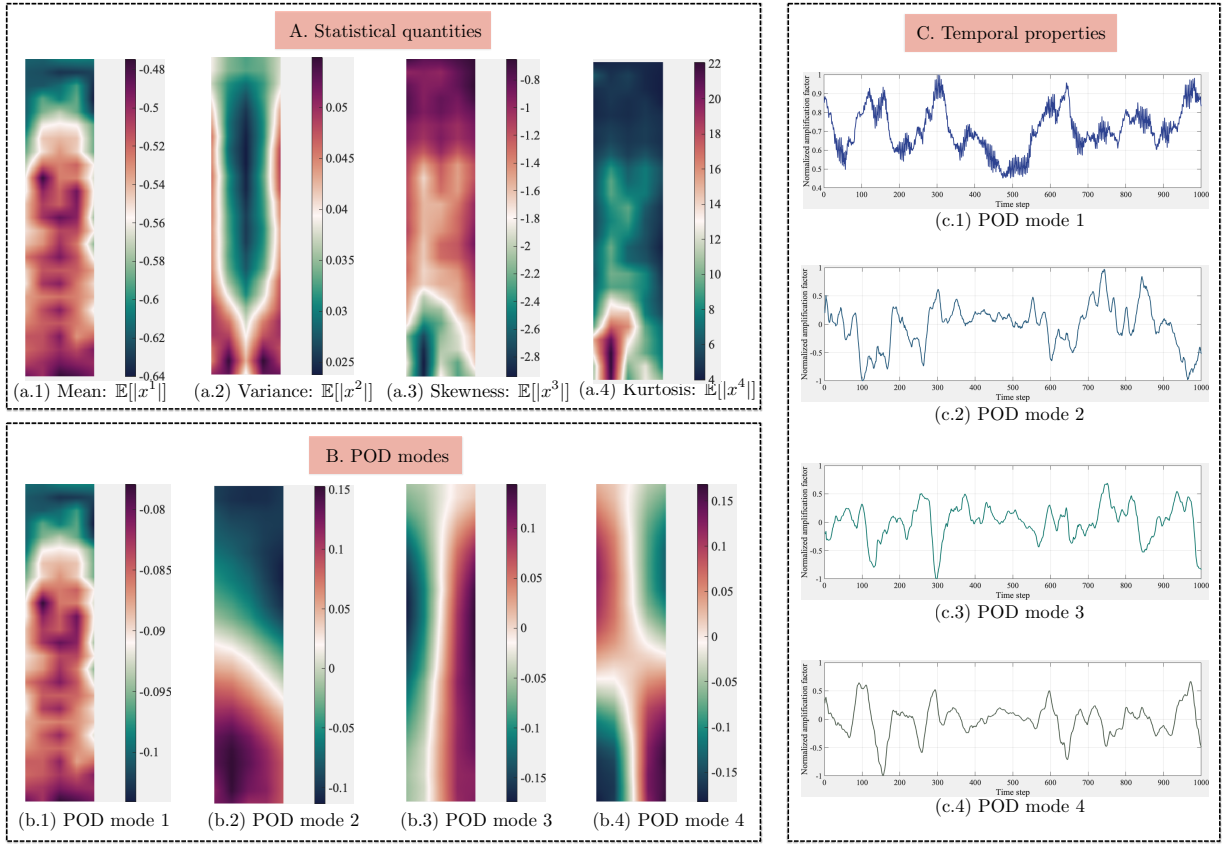


Figure 14: Leeward scenario: the decomposed spatial and temporal tensor by the POD algorithm.

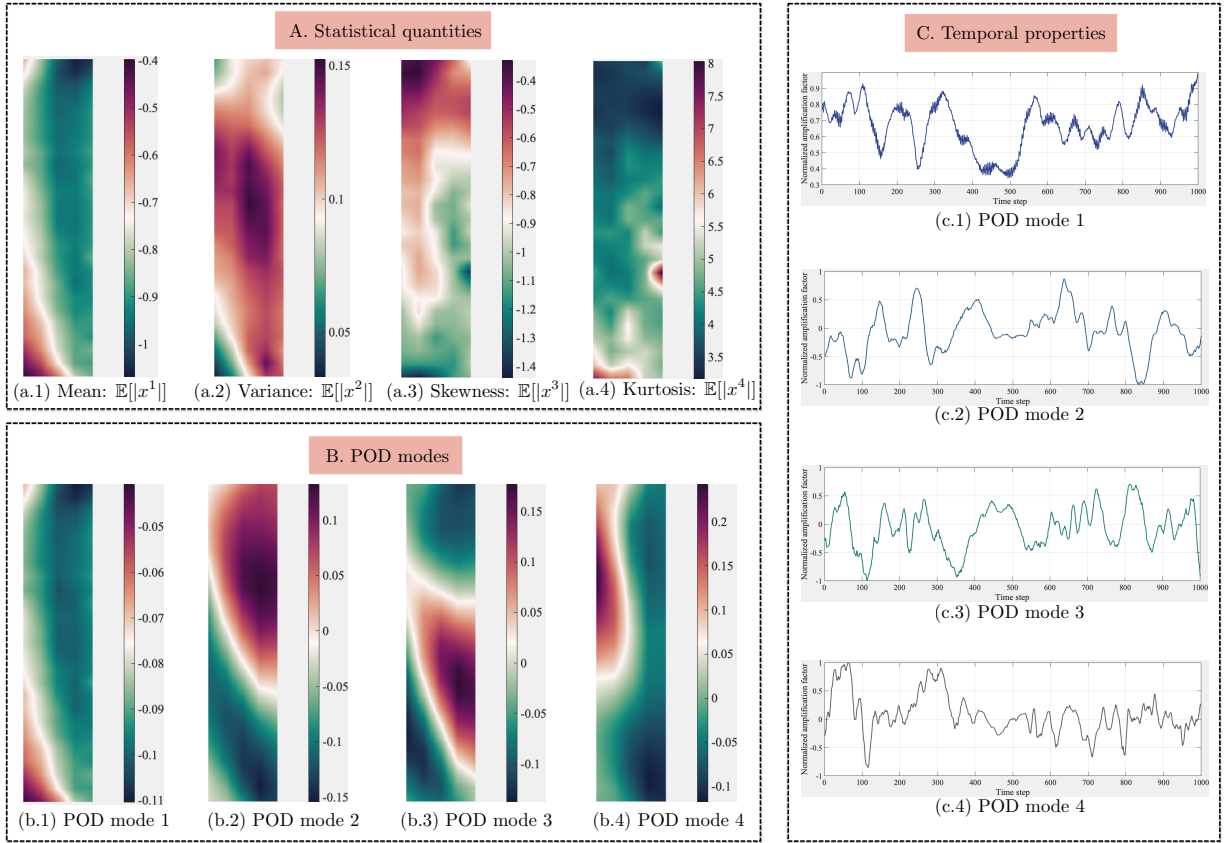
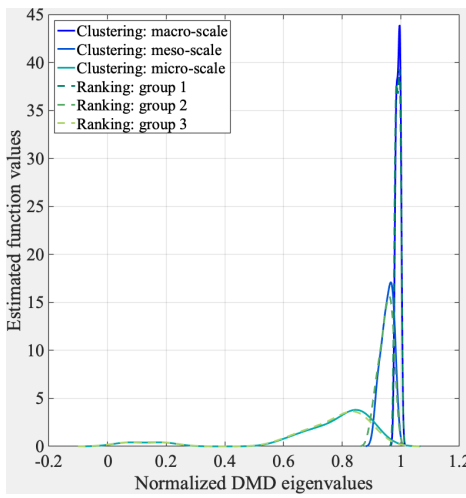
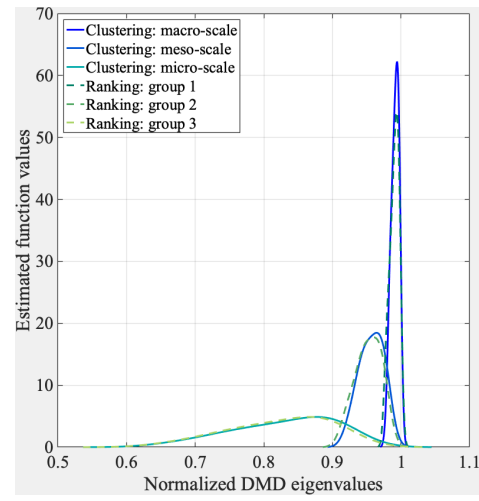


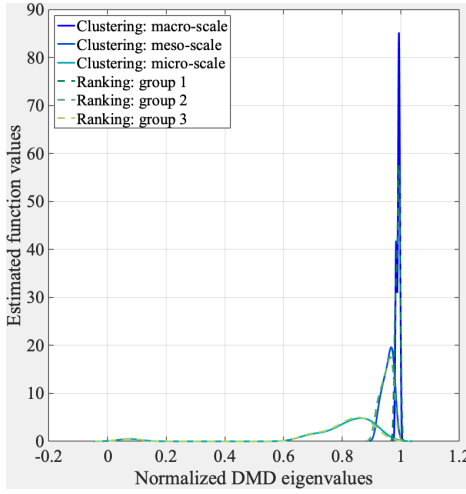
Figure 15: Rightside scenario: the decomposed spatial and temporal tensor by the POD algorithm.



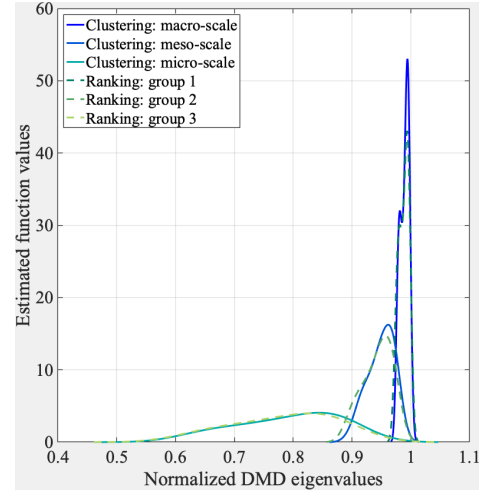
(a.1) Windward: distribution of DMD eigenvalues



(a.2) Leftside: distribution of DMD eigenvalues

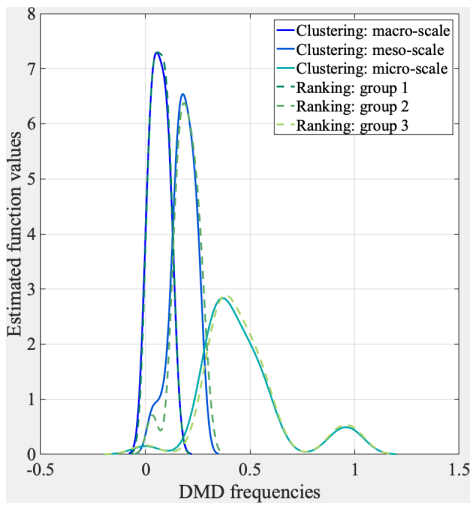


(a.3) Leeward: distribution of DMD eigenvalues

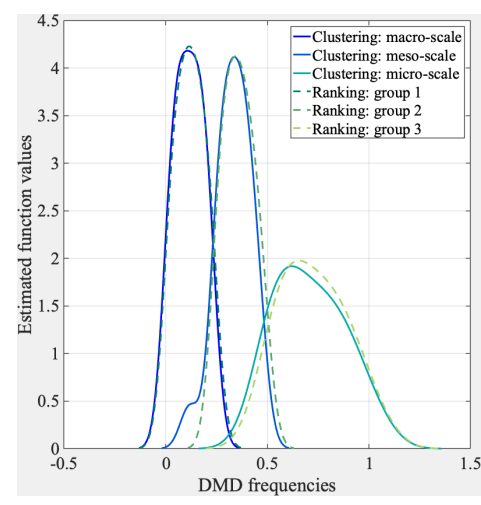


(a.4) Rightside: distribution of DMD eigenvalues

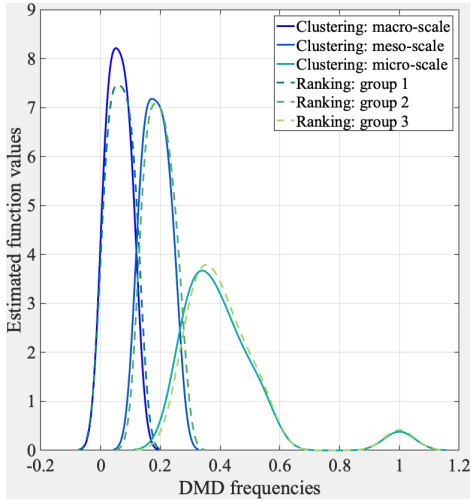
Figure 16: Distributions of clustered eigenvalues



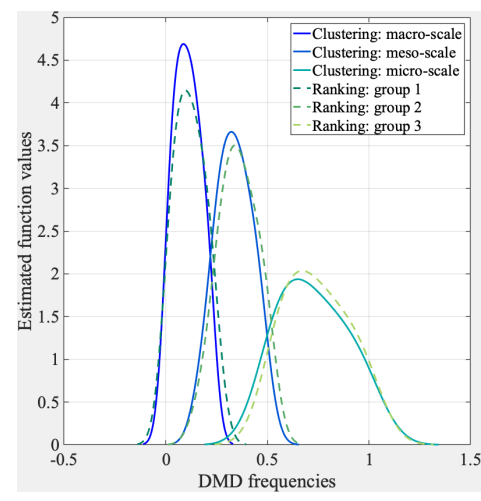
(a.1) Windward: distribution of DMD frequencies



(a.2) Leftside: distribution of DMD frequencies



(a.3) Leeward: distribution of DMD frequencies



(a.4) Rightside: distribution of DMD frequencies

Figure 17: Distributions of clustered frequencies

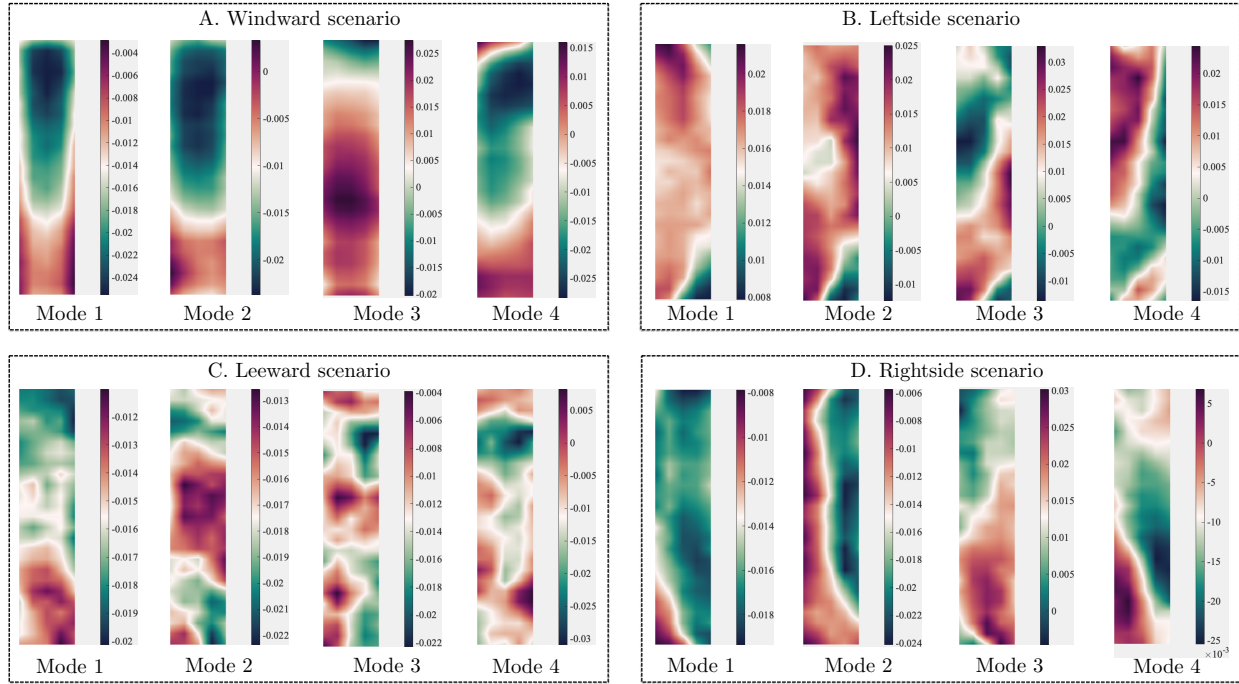


Figure 18: Macro-scale DMD modes.